What's the difference between Aquasonic® 100 and those other gels?

Clarity, reliability, and economy.

Aquasonic 100
Ultrasound Transmission Gel

The clarity that sonographers have counted on for over sixty years.

Purchasing that other gel seemed like a cost-conscious move, right? After all, while sitting on the shelf all gels are equal. But after three or four extra applications, those other gels aren't so cheap anymore.

Consider the superior formulation of Aquasonic 100 Ultrasound Transmission Gel. Aquasonic 100 aids in producing consistent, high-quality images, and since it won't dry out like other gels, it's cost-effective with each and every application. No wonder Aquasonic is the overwhelming choice of clinicians and ultrasound equipment manufacturers worldwide.

If you're currently using another ultrasound gel and would like to try Aquasonic 100, visit **www.parkerlabs.com**. We'll send you a small sample that will go a long way.

ISO 13485:2016

PARKER Parker Laboratories, Inc. | **The sound choice in patient care.™** | 973.276.9500 | parkerlabs.com

AD-01-1 REV 3

Diagnostic Performance of Multimodal Sound Touch Elastography for Differentiating Benign and Malignant Breast Masses

Fajin Dong, MD, Huaiyu Wu, MD*, Lei Zhang, MD, Hongtian Tian, MD, Weiyu Liang, MD, Xiuyin Ye, MD, Yan Liu, MD, Jinfeng Xu, PhD*

**These authors share first authorship*
Received July 19, 2018, from the Department of Ultrasound, Second Clinical College of Jinan University, Shenzhen People's Hospital, Shenzhen, China (F.D., H.W., L.Z., H.T., W.L., 9 X.Y., J.X.); and The Key Laboratory of Cardiovascular Remodeling and Function Research, Chinese Ministry of Education and Chinese Ministry of Health, and The State and Shandong Province Joint Key Laboratory of Translational Cardiovascular Medicine, Qilu Hospital of Shandong University, Jinan, China (Y.L.). Manuscript accepted for publication November 15, 2018.

This project was supported by The Clinical Project of Shenzhen People's Hospital (No. SYLY201702).

Address correspondence to Yan Liu The Key Laboratory of Cardiovascular Remodeling and Function Research, Chinese Ministry of Education and Chinese Ministry of Health, and The State and Shandong Province Joint Key Laboratory of Translational Cardiovascular Medicine, Qilu Hospital of Shandong University, No. 107, Wenhuaxi Road, Jinan, 250012, China. E-mail: 200962000811@sdu.edu.cn, Jinfeng Xu, Department of Ultrasound, Second Clinical College of Jinan University, Shenzhen People's Hospital, Shenzhen, 518020, China. E-mail: xujinfeng@yahoo.com

Abbreviations
ARFI, acoustic radiation force impulse; AUC, area under the curve; BC, breast cancer; BI-RADS, Breast Imaging Reporting and Data System; C, shear wave; CI, confidence interval; DORs, diagnostic odds ratios; E, Young's modulus; G, shear modulus; LR–, negative likelihood ratio; LR+, positive likelihood ratio; PLR+, pooled positive likelihood ratio; PLR–, pooled negative likelihood ratio; P-Sen, pooled sensitivity; P-Spe, pooled specificity; ROC, receiver operating characteristic; ROIs, regions of interest; Sen, sensitivity; Spe, specificity; STE, Sound Touch Elastography; SWE, shear wave elastography

doi:10.1002/jum.14915

Objectives—Evaluating the value of screening breast masses by separate or combined use of multimodal Sound Touch Elastography.

Methods—Women with 159 masses (mean size, 14.86 ± 6.57 mm; range, 5.30–30.00 mm) were enrolled in the study. The pathology results were adopted as diagnostic standards. The abilities of Young's modulus (E), shear modulus (G), and shear wave (C) to differentiate malignant and benign breast masses based on receiver operating characteristic curves were evaluated, and the optimal cutoff values were obtained. Sensitivity, specificity, positive likelihood ratio, and negative likelihood ratio were calculated. Then, the values were combined to perform an overall analysis of Sound Touch Elastography using evidence-based medicine, construct forest plots, and calculate areas under the summary receiver operating characteristic curves, pooled sensitivity, specificity, positive likelihood ratio, negative likelihood ratio, and diagnostic scores.

Results—A total of 159 masses with a mean size of 14.86 ± 6.57 mm (range, 5.30–30.00 mm) were included. For the various parameters, the diagnostic values were as follows: $G_{max} > E_{max} > C_{max} > C_{sd} > E_{sd} > G_{sd} > E_{mean} > G_{mean} > C_{mean}$. There were no significant differences in E_{min}, G_{min}, or C_{min}. When the 9 parameters were combined, the pooled sensitivity, specificity, positive likelihood ratio, negative likelihood ratio, diagnostic scores and areas under the summary receiver operating characteristic curves were 84% (95% confidence interval [CI], 79%–88%), 82% (95% CI, 80%–84%), 4.75 (95% CI, 4.15–5.43), 0.20 (95% CI, 0.15–0.25), 3.19 (95% CI, 2.84–3.54) and 90.2% (95% CI, 87%–92%), respectively.

Conclusions—Sound Touch Elastography can be recognized as a new ultrasound-based diagnostic method for differentiation between benign and malignant breast masses.

Key Words—breast cancer; diagnosis; elasticity imaging techniques; Sound Touch Elastography; ultrasound

Breast cancer (BC) is currently the most widely diagnosed cancer and the main cause of cancer death in women around the world, accounting for 23% of all cancer diagnoses (1.38 million women) and 14% of cancer deaths (458,000 women) per year.[1] Screening mammography reduces mortality from BC through early detection[2]; however, there is disagreement regarding optimal screening regimens.[3,4] Mammographic screening does not

detect all BCs, and cancers arising between tests (interval cancers) typically represent 25% to 50% of cancer cases diagnosed in women undergoing biennial screening.[5] Sonography has good sensitivity in detecting breast masses, but it has poor specificity because most solid lesions are benign lesions.[6,7]

Elastography has been widely used in the clinic for examining breast masses, and this technique is considered useful for differentiating malignant and benign masses.[8] Ultrasound shear wave elastography (SWE) enables the measurement of tissue strain, which is used to estimate lesion stiffness. BC masses tend to be stiff, whereas benign tissues or masses tend to be soft. SWE measures propagation of shear waves within tissues, quantifying stiffness in kilopascals or meters per second.[9,10]

Sound Touch Elastography (STE) has emerged as a novel elastography technique that can provide both maps of shear waves and parameters, such as Young's modulus (E, including E_{mean}, E_{max}, E_{min}, and E_{sd}), shear modulus (G, including G_{max}, G_{min}, G_{mean}, and G_{sd}) and shear wave (C, including C_{mean}, C_{max}, C_{min}, and C_{sd}), using the same ultrasound equipment. In this study, we first evaluated these parameters separately and then combined them by evidence-based medicine and used the pooled parameters to evaluate the clinical value of multimodal STE with E, C, and G parameters in differentiating malignant and benign breast masses.

The use of separated or pooled multimodal STE can help differentiate benign and malignant breast masses. The parameters E, G, and C have a high sensitivity (Sen), specificity (Spe), positive likelihood ratio (LR+), and negative likelihood ratio (LR–).

Materials and Methods

Patient Selection

This retrospective study was approved by the Institutional Review Board of our hospital, and all women provided informed consent. Assessment of ultrasound images for each lesion and for each breast was performed on the basis of the expanded 7 Breast Imaging Reporting and Data System (BI-RADS) categories: category 1, negative; category 2, benign; category 3, probably benign; category 4a, low suspicion of malignancy; category 4b, moderate suspicion of malignancy; category 4c, high suspicion of malignancy; and category 5, highly suggestive of malignancy.[11] The inclusion criteria were as follows: (1) lesions were stable when detected by sonography; (2) the size of the masses ranged from 5.00 to 30.00 mm; (3) solid or almost solid (<20% cystic) masses detected by sonography; (4) breast tissue surrounding masses at the same depth and sonographic cross-section; (5) women with a BI-RADS ultrasound category of 3, 4a, 4b, 4c, or 5; (6) no intervention or surgery on masses before ultrasound scan; and (6) surgery or biopsy performed within 1 week of ultrasound scanning. Not every lesion could be included for the women with multiple masses in this study because of the size and restrictions. If women had multiple masses, only the lesion that best satisfied the inclusion criteria was included.

Image Acquisition and Interpretation

All of the examinations were conducted by a radiologist who was blinded to the pathologic data and had more than 10 years of experience in sonography and 4 years of experience in elastography. Bilateral whole-breast screening sonography was performed using a Resona 7 ultrasound system (Mindray Medical Solutions, Shenzhen, China) equipped with an 11 L3 linear array transducer (bandwidth frequency of 3–11 MHz) and STE software, which can measure the stiffness of regions of interest (ROIs) and display the information in the form of E, G, and C using the same ultrasound equipment.

Women were in a supine position with the upper chest fully exposed. The sonographic features of the morphologic characteristics, size, boundary, echo, color Doppler feature, and BI-RADS categories of the masses were described and stored by the ultrasound machine.

After acquiring informed consent from the eligible participants, the same radiologist performed STE for the breast mass, defined as a single breast lesion on B-mode sonography for each participant with suspected cancer. Then, the radiologist switched to the STE mode, and the probe was touched lightly to the skin, and the size of the ROI was adjusted to include the lesion, with sufficient surrounding tissues in the ROI. The radiologist ensured that the maximum longitudinal section of the masses was displayed in the center of the screen, and when the left region of the dual images was nearly green (area > 95%) of ROI,

the radiologist pressed the update button to acquire the elastographic images of masses. STE images were extracted from the equipment. The masses were circled, and the E data (including E_{max}, E_{min}, E_{mean}, and E_{sd}), G data (including G_{max}, G_{min}, G_{mean}, and G_{sd}) and C data (including C_{max}, C_{min}, C_{mean}, and C_{sd}) were obtained.

Pathologic Diagnoses

All diagnoses were made by a pathologist who had 10 years of experience in the pathologic analysis of BC samples obtained using biopsy or surgery. Analyses were based on cytologic or histologic diagnoses (83 women underwent surgery, and 76 underwent biopsy).

Statistical Analysis

E data (E_{max}, E_{min}, E_{mean}, and E_{sd}), G data (G_{max}, G_{min}, G_{mean}, and G_{sd}) and C data (C_{max}, C_{min}, C_{mean}, and C_{sd}) of the STE images were recorded. The true-positive, true-negative, false-positive, and false-negative values were calculated for every method. The Kruskal-Wallis nonparametric test was used to determine significant differences in the E, G, and C data between benign and malignant masses. The abilities of E, G, and C to differentiate malignant from benign masses were evaluated by receiver operating characteristic (ROC) curve analysis. The optimal cutoff values were obtained using the Youden index (sensitivity + specificity – 1) from the ROC curves. Sen, Spe, LR+, LR–, and diagnostic odds ratios (DORs) were calculated with the chi-square test. A *P* value less than .05 was considered statistically significant. Then, the values were pooled together to perform an overall analysis of STE using evidence-based medicine, construct forest plots, and calculate the areas under the summary ROC curves. Pooled Sen, Spe, LR+, LR- (P-Sen, P-Spe, PLR+ and PLR-, respectively) and DORs were also calculated. The above data were analyzed with statistical software Stata 14.0 for Mac (Stata Corp, College Station, TX) and GraphPad Prism 6.0 for Mac (GraphPad Software, Inc., La Jolla, CA).

Figure 1. Images showing a BC lesion in a 55-year-old woman. **A, B,** The B- and color-mode images show a hypoechoic lesion (size, 0.94*0.71 cm) by sonography with no evidence of blood. **C,** The pathology results confirmed that the lesion was invasive lobular carcinoma. **D, E,** The lesion was evaluated by STE. The green region in D is for quality control; the greener the area, the better the obtained standard elastography image is. **E,** Quantitative Sound Touch Elastography parameters E, G, and C were measured by drawing a region of interest around the nodule to encompass the maximum area without including the tissue outside the nodule displayed on the B-mode image.

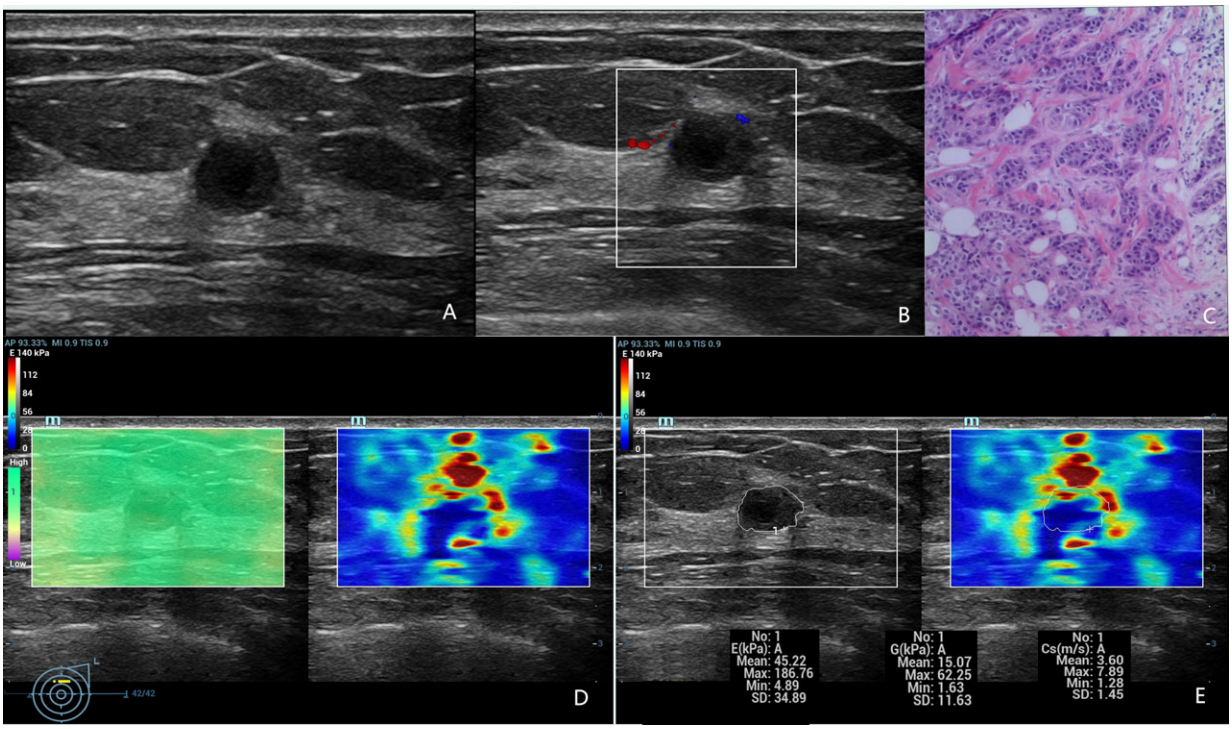

Results

Between June 2016 and December 2017, 173 women referred for ultrasound examinations were recruited in this study. Among them, 6 women had masses measuring larger than 30 mm; 8 women were lost during follow-up, and no pathologic diagnosis was available, and thus, these women were excluded from this study. The remaining 159 women (mean age, 40.36 ± 11.74 years; range, 28–79 years) with 159 masses were enrolled in the study. The 32 women with BC had a mean age of 49.34 ± 2.39 years (range, 29–91 years), and the 127 women with benign masses had a mean age of 38.10 ± 0.90 years (range, 19–65 years). The

Figure 2. Images showing a breast cancer lesion in a 35-year-old woman. **A, B,** The B- and color-mode images show a hypoechoic lesion (size, 1.41*0.75 cm) by sonography with no evidence of blood. **C,** The pathology results confirmed that the lesion was a fibroadenoma. **D, E,** The lesion was evaluated by Sound Touch Elastography. The green region in D is for quality control; the greener the area, the better the obtained standard elastography image is. **E,** Quantitative Sound Touch Elastography parameters E, G, and C were measured by drawing a region of interest around the nodule to encompass the maximum area without including the tissue outside the nodule displayed on the B-mode image.

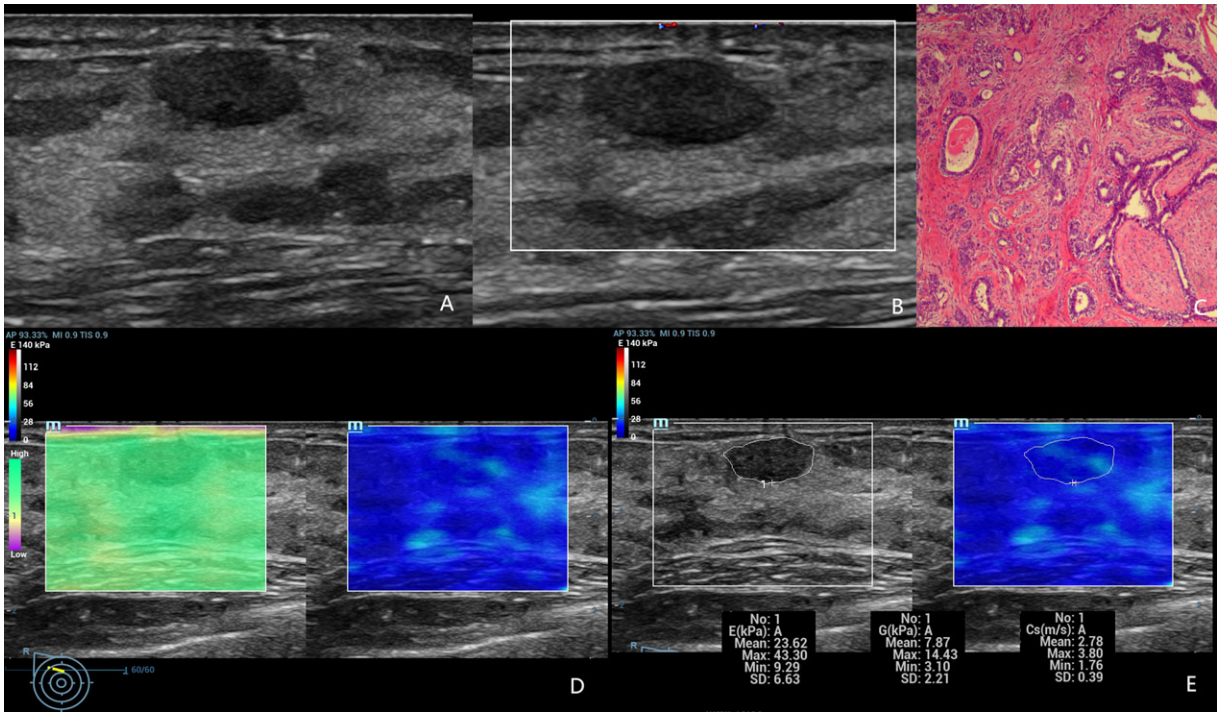

Table 1. The E Measurements of Benign and Malignant Nodules

Lesion		Max	Min	Mean ± SD	*P* Value	Cutoff	AUC	SEN	SPE	LR+	LR–
E_{mean}	Benign	96.80	7.17	24.43 ± 1.46	.0001	31.58	85.49%	81.25%	80.31%	4.13	0.23
	Maligant	109.71	22.13	46.23 ± 3.84							
E_{max}	Benign	347.84	11.24	76.89 ± 5.92	.0001	118.7	91.26%	84.38%	84.25%	5.36	0.19
	Maligant	399.82	54.59	228.0 ± 17.07							
Emin	Benign	32.05	0.03	6.44 ± 0.39	.2446	...	...	...	...	...	...
	Maligant	26.64	0.00	5.31 ± 1.15							
E_{sd}	Benign	52.69	1.54	11.67 ± 0.87	.0001	18.10	89.74%	87.50%	82.68%	5.05	0.15
	Maligant	61.89	9.61	30.86 ± 2.51							

AUC indicates area under the receiver operating characteristic curve; LR–, negative likelihood ratio; LR+, positive likelihood ratio; Sen, sensitivity; and Spe, specificity.

159 masses in these women had a mean size of 14.86 ± 6.57 mm (range, 5.30–30.00 mm), satisfying the inclusion criteria. The malignant masses had a mean size of 19.68 ± 1.35 mm (range, 6.50–30.00 mm), and the benign masses had a mean size of 13.65 ± 0.50 mm (range, 5.30–30.00).

Finally, 29 women with invasive ductal carcinoma, 1 patient with invasive lobular carcinoma, 2 women with ductal carcinomas in situ. One hundred seventeen women with fibroadenomas, 3 women with intraductal papilloma, 6 women with sclerosing adenosis, and 1 patient with hamartoma were enrolled in this study.

Figure 3. Summary ROC curves of E (including E_{max}, E_{mean}, and E_{sd}), G (including G_{max}, G_{mean}, and G_{sd}) and C (C_{max}, C_{mean}, and C_{sd}) parameters.

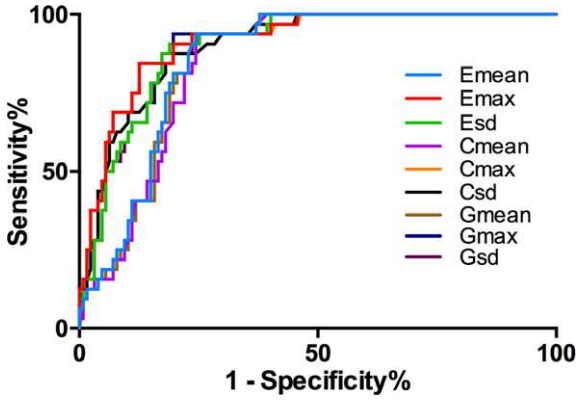

E Measurements of Benign and Malignant Masses

The stiffness of the masses is shown in Figures 1 and 2. Blue in the upper left indicates the softest, and red indicates the hardest regions of the lesion. In this study, all 32 malignant masses displayed a reddish periphery (red rimlike) and a yellow or yellow-green region in the middle, while the 132 benign lesion displayed colors similar to those of surrounding tissues and were either green or yellow and had no red regions suggestive of malignancy.

Figure 4. Distribution of E_{mean}, E_{max}, and E_{sd} between malignant and benign breast lesions.

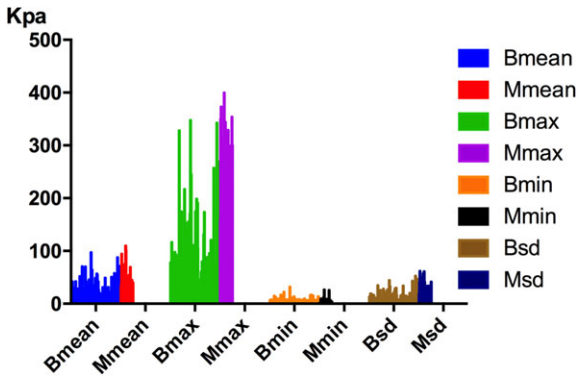

Figure 5. Distribution of G_{mean}, G_{max}, and G_{sd} between malignant and benign breast lesions.

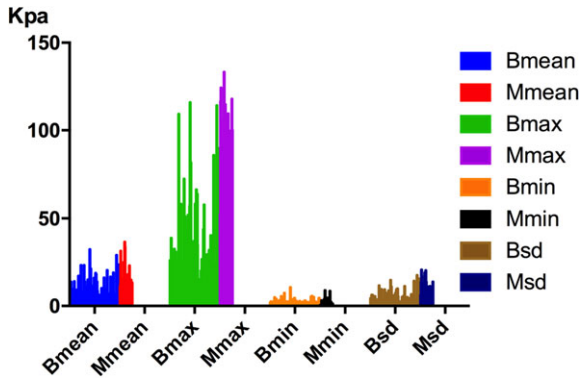

Table 2. The G Measurements of Benign and Malignant Nodules

Lesion		Max	Min	Mean ± SD	*P* Value	Cutoff	AUC	SEN	SPE	LR+	LR–
G_{mean}	Benign	8.11	1.54	8.20 ± 0.50	.0001	10.53	85.05%	81.25%	79.53%	3.97	0.24
	Maligant	36.57	7.38	15.45 ± 1.28							
G_{max}	Benign	10.77	1.94	25.63 ± 1.97	.0001	39.57	91.39%	84.38%	84.25%	5.36	0.18
	Maligant	133.27	18.86	76.13 ± 5.66							
G_{min}	Benign	3.27	0.10	2.15 ± 0.13	.4507	...	...	...	...	...	...
	Maligant	8.88	0.00	1.90 ± 0.39							
G_{sd}	Benign	1.66	0.14	3.90 ± 0.29	.0001	6.03	89.54%	87.50%	82.68%	5.05	0.15
	Maligant	20.63	3.20	10.27 ± 0.84							

AUC indicates area under the receiver operating characteristic curve; LR–, negative likelihood ratio; LR+, positive likelihood ratio; Sen, sensitivity; and Spe, specificity.

The E measurements of benign and malignant breast masses are shown in Table 1. E_{max}, E_{mean}, and E_{sd} were significantly higher in malignant masses than in benign masses ($P < .0001$). There were no significant differences in E_{min} ($P = .2446$). The ROC curves of the other 3 E parameters are shown in Figure 4. Compared with the other E parameters, E_{max} with the optimal cutoff value of 118.7 kPa had the highest area under the curve (AUC), which was 84.38% (95% confidence interval [CI], 79.77%–91.22%). Based on this cutoff value, the diagnostic Sen, Spe, LR+, and LR– were 84.38%, 84.25%, 5.36, and 0.19, respectively (Table 1). The other 2 E parameters, E_{mean} and E_{sd}, had cutoff values of 31.58 kPa and 18.10 kPa and AUCs of 85.49% (95% CI, 86.46%–96.07%) and 89.74% (95% CI, 84.76%–94.72%), respectively. The details are shown in Table 1 and Figure 4.

G Measurements of Benign and Malignant Masses

The stiffness of the masses is indicated by the same color as for E. The G measurements of benign and malignant breast masses are shown in Table 2. G_{max}, G_{mean}, and G_{sd} were significantly higher in malignant masses than in benign masses ($P < .0001$). There were no significant differences in G_{min} ($P = .4507$). The ROC curves of the other 3 G parameters are shown in Figure 3. Compared with the other G parameters, G_{max} with the optimal cutoff value of 39.57 kPa had the highest AUC, which was 91.39% (95% CI, 86.63%–96.15%). Based on this cutoff value, the diagnostic Sen, Spe, LR+, and LR– were 84.38%, 84.25%, 5.36, and 0.19, respectively (Table 2). The other two G parameters, G_{mean} and G_{sd}, had cutoff values of 10.53 kPa and 6.03 kPa and AUCs of 85.05% (95% CI, 79.25%–90.86%) and 89.54% (95% CI, 84.51%–94.57%), respectively. The details are shown in Table 2 and Figure 5.

C Measurements of Benign and Malignant Masses

The stiffness of the masses is indicated by the same color as for E. The C measurements of benign and malignant breast masses are shown in Table 3. C_{max}, C_{mean}, and C_{sd} were significantly higher in malignant masses than in benign masses ($P < .0001$). There were no significant differences in C_{min} ($P = .4372$). The ROC curves of the other 3 C parameters are shown in Figure 3. Compared with the other C parameters, C_{max} with the optimal cutoff value of 6.84 m/s had the highest AUC, which was 91.24% (95% CI, 86.42%–96.06%). Based on this cutoff value, the diagnostic Sen, Spe, LR+, and LR– were 84.38%, 87.40%, 6.70, and 0.18, respectively (Table 3). The other 2 C parameters, C_{mean} and C_{sd}, had cutoff values of 3.14 m/s and 0.87 m/s and AUCs of 84.49% (95% CI, 78.59%–90.39%) and 89.90% (95% CI, 84.84%–94.96%), respectively. The details are shown in Table 3 and Figure 6.

Figure 6. Distribution of C_{mean}, C_{max}, and C_{sd} between malignant and benign breast lesions.

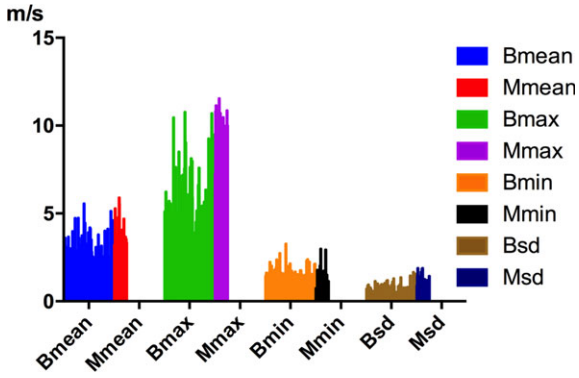

Table 3. The C measurements of Benign and Malignant Nodules

Lesion		Max	Min	Mean ± SD	*P* Value	Cutoff	AUC	SEN	SPE	LR+	LR–
C_{mean}	Benign	5.56	1.54	2.66 ± 0.07	.0001	3.14	84.49%	81.25%	77.95%	3.69	0.24
	Maligant	5.89	2.66	3.65 ± 0.14							
C_{max}	Benign	10.77	1.94	4.71 ± 0.17	.0001	6.84	91.24%	84.38%	87.40%	6.70	0.18
	Maligant	11.54	4.34	8.50 ± 0.35							
C_{min}	Benign	3.27	0.10	1.39 ± 0.04	.117	…	…	…	…	…	…
	Maligant	2.98	0.00	1.09 ± 0.14							
C_{sd}	Benign	1.66	0.14	0.60 ± 0.03	.0001	0.87	89.90%	84.38%	81.89%	4.66	0.19
	Maligant	1.88	0.55	1.16 ± 0.06							

AUC indicates area under the receiver operating characteristic curve; LR–, negative likelihood ratio; LR+, positive likelihood ratio; Sen, sensitivity; and Spe, specificity.

Pooled E, G, and C Measurements of Benign and Malignant Masses

We combined the 9 parameters for E, G, and C using the Midas module of Stata 14.0, equipped with the bivariate mixed-effects regression model developed by van Houwelinge and modified for the synthesis of diagnostic test data,[12,13] to pool the statistical indexes and draw statistical graphs. The P-Sen, P-Spe, PLR+, PLR–, and DORs with corresponding 95% CIs and areas under the summary ROC curves were used to examine the diagnostic accuracy. As shown in Figure 8 A and B, significant heterogeneity was detected in P-Sen (I^2 = 0%, Q = 1.31) and P-Spe (I^2 = 0.00%, Q = 5.64). The P-Sen, P-Spe, PLR+, PLR–, DORs, and areas under the summary ROC curves were 84% (95% CI, 79%–88%), 82% (95% CI, 80%–84%), 4.75 (95% CI, 4.15–5.43), 0.20 (95% CI, 0.15–0.25), 3.19 (95% CI, 2.84–3.54), and 90.2% (95% CI, 87%–92%), respectively (Table 4 and Figures 7 and 8).

Figure 8. Summary receiver operating characteristic curves of EI, G_{max}, G_{mean}, and G_{sd} with 95% CIs. CIs indicates confidence intervals.

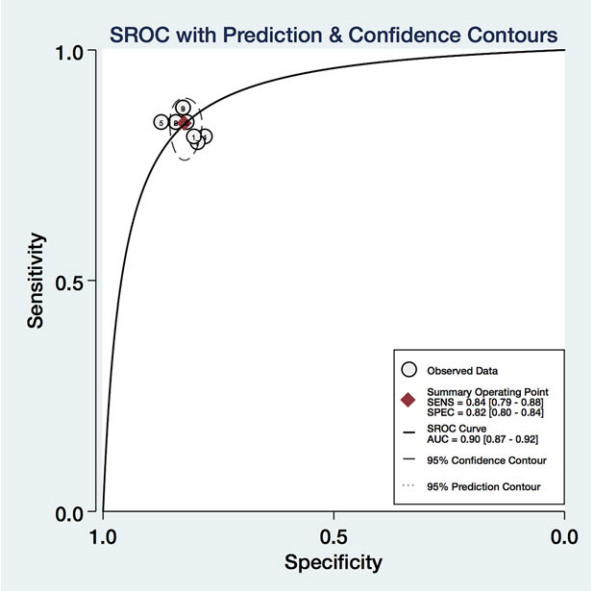

Figure 7. Pooled Sen **(A),** Spe **(B),** LR+ **(C),** LR– **(D),** DOR **(E),** and OR **(F)** of EI, G_{max}, G_{mean}, and G_{sd} with 95% CIs. CIs indicates confidence intervals; DOR, diagnostic odds ratio; LR–, negative likelihood ratio; LR+, positive likelihood ratio; Sen, sensitivity; and Spe, specificity.

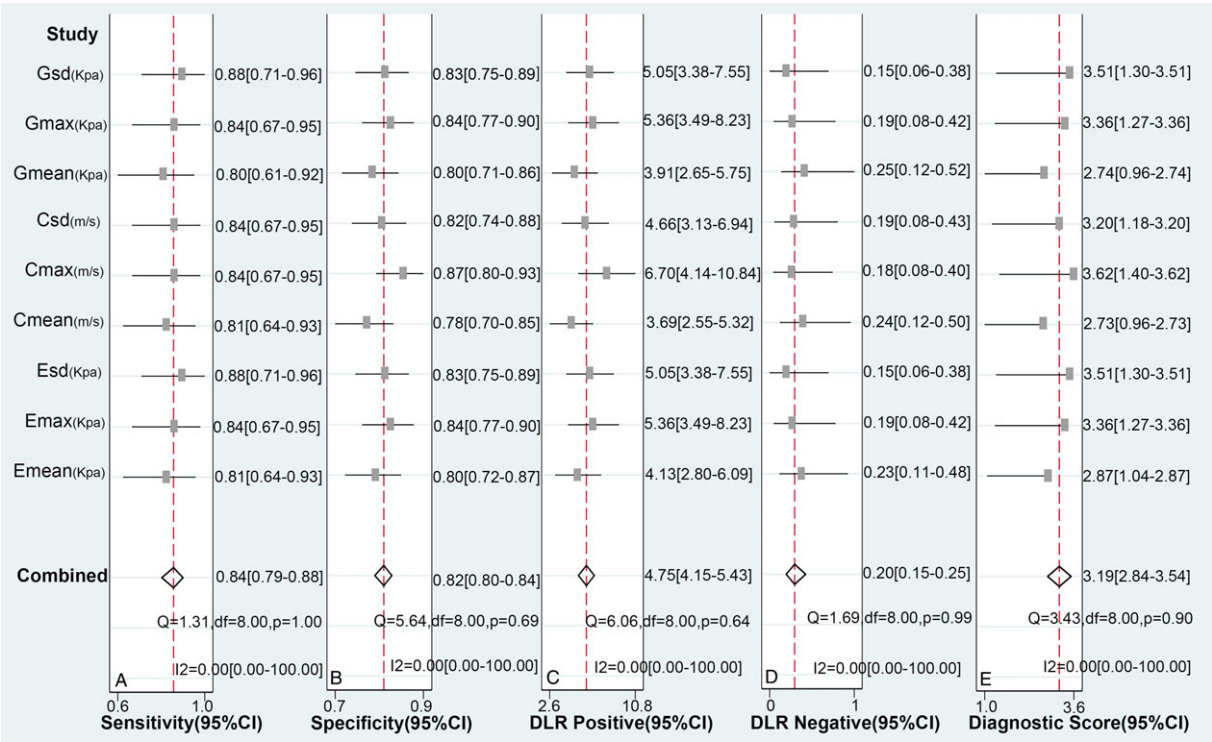

Discussion

Generally, BC tissues are harder than surrounding normal breast tissues. This property enables several examinations, for example, palpation, which is widely used as a part of the clinical appraisal of irregularities in the breast, and elastography. The theory underlying elastography is that tissue pressure produces strain (dislodging) inside the tissue and that the strain is smaller in harder tissues than in softer tissues. Thus, by estimating the tissue strain using pressure, we can evaluate tissue hardness, which might be helpful for diagnosing BC.[14] Invasive BC masses are stiffer than normal tissues or benign masses[15] and often present larger areas of stiffness on ultrasound images.[14,16]

During the invasive growth of BC, internal necrosis is often accompanied by changes in shear wave elasticity. This is called the "stiff rim" sign, consistent with relevant reports.[17] An increase in the stiffness of surrounding tissues may indicate that cancer cells have invaded these tissues surrounding the tumor.[14] Studies have shown that cancer cell infiltration around the tumor is an independent prognostic factor for predicting tumor recurrence and patient death.[18]

Elastography, including strain imaging, acoustic radiation force impulse (ARFI) imaging and SWE, has been recognized as a useful technique for evaluating breast masses and assesses stiffness to provide color images and digital data.[19] For the strain elasticity score, an optimal cutoff value between 3 and 4 was used, and the Sen and Spe of elastography were 86.5% and 89.8%, respectively.[14] By selecting a lesion cutoff value of 3.31 m/s on ARFI images, Ianculescu et al[20] obtained 80.4% Sen and 73% Spe. For SWE, the optimal cutoff of the mean shear wave elasticity was 80.17 kPa, and the Sen and Spe were 88.8% and 84.9%, respectively.[21]

Some published meta-analyses have evaluated the stiffness of breast masses using strain, ARFI, and SWE. Sadigh et al[22] performed a systematic review of the strain ratio and length ratio for differentiating malignant and benign breast masses. Nine studies with 2087 breast masses (667 BC masses) were included, and the P-Sen, P-Spe, PLR+, and PLR– were 88% (95% CI, 84%–91%), 83% (95% CI, 78%–88%), 5.57 (95% CI, 3.85–8.01), and 0.14 (95% CI, 0.09–0.20), respectively. Another systematic review[23] evaluated the diagnostic efficacy of ARFI. A total of 15 studies were included, which contained 1873 breast masses (743 BC masses). The P-Sen and P-Spe for Virtual Touch Imaging were 91.3% (95% CI, 77.9%–96.9%) and 87.1% (95% CI, 77.3%–93.0%), respectively. The P-Sen and P-Spe for Virtual Touch Quantification were 84.9% (95% CI, 80.5%–88.4%) and 88.9% (95% CI, 77.1%–95.0%), respectively, and for pooled Virtual Touch Imaging and Virtual Touch Quantification, the P-Sen and P-Spe were 93.5% (95% CI, 89.2%–96.1%) and 88.1% (95% CI, 81.8%–92.4%), respectively. Another systematic review of SWE[24] included 33 studies, with a total of 5838 masses (2093 BC masses). The P-Sen and P-Spe were 88.6% (95% CI, 85.8%–90.9%) and 86.6% (95% CI, 83.3%–89.4%), respectively.

STE is a novel elastography technique that can provide E (including E_{max}, E_{mean}, E_{min}, and E_{sd}), C (including C_{max}, C_{mean}, C_{min}, and C_{sd}) and G (including G_{max}, G_{mean}, G_{min}, and G_{sd}) data, as well as the strain ratio using the same ultrasound equipment. The inversion algorithm of the 3 parameters is based on the shear wave propagation equation in isotropic, homogeneous solids[25–27] as follows: $G = \rho*C^2$ and $E = 3*\rho*C^2$, where G is the shear modulus, E is the Young's modulus, C is the shear wave velocity, and ρ is the density. This equation can be extended to cases of heterogeneous media in which the variations in G are minimal, for example, in the human body, where the tissues are different. However, considering the difference in the viscosity coefficient of human tissues, there is some relative

Table 4. The Statistical Results of Benign and Malignant Lesions

Parameters	E_{mean}	E_{max}	E_{sd}	G_{mean}	G_{max}	G_{sd}	C_{mean}	C_{max}	C_{sd}
TP	26	27	28	26	27	28	26	27	27
FP	25	20	22	26	20	22	28	16	23
FN	6	5	4	6	5	4	6	5	5
TN	102	107	105	101	107	105	99	111	104

FN indicates false-negative; FP, false-positive, TN, true-negative; and TP, true-positive.

inaccuracy in the conversion process, and the equations change to $G \approx \rho^*C^2$, $E \approx 3^*\rho^*C^2$, and $E \approx 3^*G$. Therefore, in this retrospective study, we evaluated these parameters separately. The sequence of these parameters for distinguishing benign and malignant breast masses is as follows: $G_{max} > E_{max} > C_{max} > C_{sd} > E_{sd} > G_{sd} > E_{mean} > G_{mean} > C_{mean}$. These parameters showed the value of screening BCs. To know the value when using these parameters together, we combined these parameters, and the P-Sen, P-Spe, PLR+, and PLR– were 84% (95% CI, 79%–88%), 82% (95% CI, 80%–84%), 4.75 (95% CI, 4.15–5.43) and 0.20 (95% CI, 0.15–0.25), respectively (Figure 8). The combined parameters also showed the clinical value of evaluating BCs. These results are similar to those of previous studies on elastography.

Our study has some limitations. First, this is a retrospective research, and the size of the patient sample small. Second, the STE technique also provides information on the periphery surrounding the ROI, due to the limitation in layout. Nevertheless, we will continue our analysis in subsequent papers, because this information is still valuable. Third, different elastography systems from different manufacturers may result in differences in values and thus need standardization.

Conclusion

This study investigates the value of STE technology for screening breast masses. We compared single and combined parameters and concluded that STE could provide both elastography images and large amounts of data, including E, G, and C, and due to the high Sen, Spe, LR+, LR–, and AUCs, STE can be used a tool to evaluate benign and malignant breast masses. In the future, we will do further study to generate a more exhaustive and practical diagnostic report.

References

1. Jemal A, Bray F, Center MM, et al. Global cancer statistics. *CA Cancer J Clin* 2011; 61:69–90.
2. Nelson HD, Tyne K, Naik A, et al. Screening for breast cancer: systematic evidence review update for the US Preventive Services Task Force. *Ann Intern Med* 2009; 151:727–W242.
3. Marmot MG. Sorting through the arguments on breast screening. *JAMA* 2013; 309:2553–2554.
4. Esserman L, Shieh Y, Thompson I. Rethinking screening for breast cancer and prostate cancer. *JAMA* 2009; 302:1685–1692.
5. Coldman AJ, Phillips N. Breast cancer survival and prognosis by screening history. *Br J Cancer* 2014;110:556.
6. Goddi A, Bonardi M, Alessi S. Breast elastography: a literature review. *J Ultrasound Med* 2012; 15:192–198.
7. Saarenmaa I, Salminen T, Geiger U, et al. The effect of age and density of the breast on the sensitivity of breast cancer diagnostic by mammography and ultrasonography. *Breast Cancer Res Treat* 2001; 67:117–123.
8. Garra BS, Cespedes EI, Ophir J, et al. Elastography of breast lesions: initial clinical results. *Radiology* 1997; 202:79–86.
9. Berg WA, Cosgrove DO, Doré CJ, et al. Shear-wave elastography improves the specificity of breast US: the BE1 multinational study of 939 masses. *Radiology* 2012; 262: 435–449.
10. Cosgrove DO, Berg WA, Doré CJ, et al. Shear wave elastography for breast masses is highly reproducible. *Eur Radiol* 2012; 22: 1023–1032.
11. Mendelson EB, Bohm-Velez M, Berg WA, et al. ACR BI-RADS ultrasound. In: *ACR BIRADS Atlas, Breast Imaging Reporting and Data System*. Reston, VA: American College of Radiology; 2013.
12. van Houwelingen HC, Arends LR, Stijnen T. Advanced methods in meta-analysis: multivariate approach and metaregression. *Stat Med* 2002; 21:589–624.
13. Van Houwelingen HC, Zwinderman KH, Stijnen T. A bivariate approach to meta-analysis. *Stat Med* 1993; 12:2273–2284.
14. Itoh A, Ueno E, Tohno E, et al. Breast disease: clinical application of US elastography for diagnosis. *Radiology* 2006; 239:341–350.
15. Fleury EF, Fleury JC, Piato S, et al. New elastographic classification of breast lesions during and after compression. *Diagn Interv Radiol* 2009; 15:96–103.
16. Schaefer FK, Heer I, Schaefer PJ, et al. Breast ultrasound elastography: results of 193 breast lesions in a prospective study with histopathologic correlation. *Eur J Radiol* 2011; 77:450–456.
17. Zhou J, Zhan W, Chang C, et al. Breast lesions: evaluation with shear wave elastography, with special emphasis on the "stiff rim" sign. *Radiology* 2014; 272:63–72.
18. De Mascarel I, Bonichon F, Durand M, et al. Obvious peritumoral emboli: an elusive prognostic factor reappraised. Multivariate analysis of 1320 node-negative breast cancers. *Eur J Cancer* 1998; 34: 58–65.
19. Evans A, Whelehan P, Thomson K, et al. Quantitative shear wave ultrasound elastography: initial experience in solid breast masses. *Breast Cancer Res* 2010; 12:R104.
20. Ianculescu V, Ciolovan LM, Dunant A, et al. Added value of Virtual Touch IQ shear wave elastography in the ultrasound assessment of breast lesions. *Eur J Radiol* 2014; 83:773–777.
21. Chang JM, Moon WK, Cho N, et al. Clinical application of shear wave elastography (SWE) in the diagnosis of benign and malignant breast diseases. *Breast Cancer Res Treat* 2011; 129:89–97.

22. Sadigh G, Carlos RC, Neal CH, et al. Accuracy of quantitative ultrasound elastography for differentiation of malignant and benign breast abnormalities: a meta-analysis. *Breast Cancer Res Treat* 2012;134: 923–931.
23. Liu B, Zheng Y, Shan Q, et al. Elastography by acoustic radiation force impulse technology for differentiation of benign and malignant breast lesions: a meta-analysis. *J Med Ultrason* 2016; 43:47–55.
24. Liu B, Zheng Y, Huang G, et al. Breast lesions: quantitative diagnosis using ultrasound shear wave elastography—a systematic review and meta-analysis. *Ultrasound Med Biol* 2016;42:835–847.
25. Ophir J, Cespedes I, Ponnekanti H, et al. Elastography: a quantitative method for imaging the elasticity of biological tissues. *Ultrason Imaging* 1991; 13:111–134.
26. Dutt V, Kinnick RR, Greenleaf JF. Acoustic shear wave displacement measurement using ultrasound. In: *1996 Ultrasonics Symposium. Proceedings*. Vol. 2. San Antonio, TX, 1996; 1185–1188.
27. Sandrin L, Tanter M, Catheline S, et al. Shear modulus imaging with 2-D transient elastography. *IEEE Trans Ultrason Ferroelectr Freq Control* 2002;49:426–435.